TITLE: Pretectal projections to the oculomotor cerebellum in hummingbirds (Calypte anna), zebra finches (Taeniopygia guttata) and pigeons (Columba livia)

AUTHORS: Andrea H. Gaede, Cristian Gutierrez-Ibanez, Melissa S. Armstrong, Douglas L. Altshuler, Douglas R. Wylie

JOURNAL: Journal of Comparative Neurology

PUBLISHER: Wiley

PUBLICATION DATE: 5 April 2019

DOI: https://doi.org/10.1002/cne.24697

Pretectal projections to the oculomotor cerebellum in hummingbirds (*Calypte anna*), zebra finches (*Taeniopygia guttata*) and pigeons (*Columba livia*)

Journal:	*Journal of Comparative Neurology*
Manuscript ID	JCN-18-0296.R1
Wiley - Manuscript type:	Research Article
Keywords:	optic flow, accessory optic system, pretectum, avian vision, visual motion processing

Pretectal projections to the oculomotor cerebellum in hummingbirds (*Calypte anna*), zebra finches (*Taeniopygia guttata*) and pigeons (*Columba livia*)

Andrea H. Gaede[1,2]*, Cristian Gutierrez-Ibanez[1]*, Melissa S. Armstrong[2], Douglas L. Altshuler[2#], Douglas R. Wylie[1#]

Keywords: optic flow, accessory optic system,

Support: This research was supported by funding to D.R.W. and D.L.A. from the Natural Sciences and Engineering Research Council of Canada (NSERC)

*These authors contributed equally and should be considered co-first authors

[#]Co-principal investigators

Corresponding authors: Douglas L. Altshuler (doug@zoology.ubc.ca) and Douglas R. Wylie (dwylie@ualberta.ca)

Abstract:

In birds, optic flow is processed by a retinal-recipient nucleus in the pretectum, the nucleus lentiformis mesencephali (LM), which then projects to the cerebellum, a key site for sensorimotor integration. Previous studies have shown that the LM is hypertrophied in hummingbirds, and that LM cell response properties differ between hummingbirds and other birds. Given these differences in anatomy and physiology, we ask here if there are also species differences in the connectivity of the LM. The LM is separated into lateral and medial subdivisions, which project to the oculomotor cerebellum and the vestibulocerebellum. In pigeons, the projection to the vestibulocerebellum largely arises from the lateral LM, and projection to the oculomotor cerebellum largely arises from the medial LM (Pakan et al., 2006). Here, using retrograde tracing, we demonstrate differences in the distribution of projections in these pathways between Anna's hummingbirds (*Calypte anna*), zebra finches (*Taeniopygia guttata*) and pigeons (*Columba livia*). In all three species, the projections to the vestibulocerebellum were largely from lateral LM. In contrast, projections to the oculomotor cerebellum in hummingbirds and zebra finches do not originate in the medial LM (as in pigeons) but instead largely arise from pretectal structures just medial, the nucleus laminaris precommissuralis and nucleus principalis precommissuralis. These species differences in projection patterns provide further evidence that optic flow circuits differ among bird species with distinct modes of flight.

1. Introduction:

Image motion across the retina due to self-motion, termed optic flow, is a critical input for visuomotor control and navigation through the environment. In all vertebrates, retinal-recipient nuclei of the accessory optic system and pretectum form visual pathways that process global visual motion (Simpson, 1984; Giolli et al., 2006). In birds, key nuclei involved in these specialized pathways include the nucleus of the basal optic root (nBOR) of the accessory optic system (Brecha et al., 1980) and the nucleus lentiformis mesencephali (LM) of the pretectum (Gamlin and Cohen, 1988a; b). In vertebrates, these pathways, or their homologues, are responsible for generating the optokinetic reflex to maintain retinal image stabilization (Waespe and Henn, 1987). Projections from the LM, nBOR, and other visual nuclei converge in the oculomotor cerebellum (folia VI-VIII) and folium IXcd of the vestibulocerebellum where sensorimotor control is coordinated (Clarke, 1977; Pakan et al., 2006).

The LM, but not other visual nuclei, is hypertrophied in hummingbirds relative to other birds (Iwaniuk and Wylie, 2007). This enlargement may represent a neural specialization related to hovering flight. Hummingbirds are very sensitive to small changes in their visual environment while hovering, and will drift to compensate for optic flow in all directions (Goller and Altshuler, 2014). In nearly all tetrapods studied to date, the typical pattern observed is that LM neurons prefer temporo-nasal (back-to-front) motion across the retina, and nBOR neurons prefer naso-temporal (front-to-back), upward or downward motion (Hoffmann and Schoppmann, 1981; Fite, 1985; Mckenna and Wallman, 1985; Winterson and Brauth, 1985; Mustari and Fuchs, 1990; Ibbotson et al., 1994; Wylie and Crowder, 2000). However, in hummingbirds, a different pattern of response properties in the LM emerged (Gaede et al., 2017). The majority of LM neurons do not prefer temporo-nasal motion; instead, there is a more uniform distribution of preferred directions, with cells preferring upward, downward, and naso-temporal motion as frequently as temporo-nasal motion (Gaede et al., 2017). Consistent with other tetrapods, there is a strong population-level preference for temporo-nasal motion among LM neurons of zebra finches and pigeons. Furthermore, hummingbird and zebra finch LM neurons prefer higher velocities of visual motion than pigeon LM neurons (Gaede et

al., 2017). This suggests a role for the LM in responding to high-speed visual motion during hovering and collision avoidance in hummingbirds.

The projection to and from both the LM and nBOR have been studied extensively in pigeons (reviewed in Wylie, 2013; Wylie et al., 2018). The projection to the vestibulocerebellum largely arises from the lateral LM, with fewer inputs from the medial LM. Conversely, the majority of LM projections to the oculomotor cerebellum originate from the medial LM, with fewer inputs from the lateral LM. Additionally, in pigeons the nBOR projects preferentially to folium IXcd of the vestibulocerebellum (Pakan et al., 2006). These two pathways of optic flow to the cerebellum of birds have been proposed to serve different functions in visuo-motor control, particularly during flight (Wylie et al., 2018). The marked differences in flight behavior between hummingbirds and other birds, and the unique characteristics of the hummingbird LM, motivated us to ask if differences in the connectivity of the LM and nBOR exist between species. We addressed this question by injecting retrograde tracers in the oculomotor cerebellum (folia VI,VII) and the vestibulocerebellum (folium IXcd) of hummingbirds, zebra finches and pigeons. We focused our analysis on projections from the accessory optic system and the pretectum.

2. Materials and Methods:

Animals.

All experimental procedures were approved by the University of British Columbia Animal Care Committee in accordance with the guidelines set out by the Canadian Council on Animal Care. Experiments were performed on four adult male Anna's hummingbirds (*Calypte anna*; caught on the University of British Columbia campus), two adult male zebra finches (*Taeniopygia guttata*; Eastern Bird Supplies, Quebec, Canada), and two adult male pigeons (*Columba livia*).

Surgery and retrograde labeling procedures.

Birds were anesthetized by intramuscular injection in the pectoral muscles with a ketamine/xylazine mixture (65 mg/kg ketamine / 8 mg/kg xylazine). Supplemental doses were administered as required. Subcutaneous injections of 0.9% saline were given to maintain fluids. Once anesthetized, hummingbirds and zebra finches were placed in a

custom-built stereotaxic frame (Herb Adams Engineering, Glendora, CA, USA) with ear bars and an adjustable beak bar suitable for both species. The head was angled downward at an angle of 45° to the horizontal plane. Bone and dura mater overlying the cerebellum were removed to expose the surface of the brain and allow access to either folia VI/VII (oculomotor cerebellum) or folium IXcd (vestibulocerebellum) with vertical penetrations. Anatomical markers on the surface of the brain were used to identify injection sites in folia VI/VII (oculomotor cerebellum) and lateral IXcd (vestibulocerebellum). Electrophysiological recordings were used to identify the medial ventral layer of folium IXcd. After identifying an injection site, a glass micropipette (tip diameter 20–30 μm) containing a retrograde tract tracer conjugated to a fluorescent dye (cholera toxin B-AlexaFluor 488 (green) or 594 (red), Invitrogen, USA) was lowered to the appropriate level to inject into the granule cell layer of the target folium. The cholera toxin-B (CTB) conjugates were injected into folium IXcd and folium VI or VII of the cerebellum using iontophoresis (+/- 4 μA, 7s on, 7s off) for 15 minutes. At the end of the injection period, the electrode was left undisturbed for 5 minutes, and then withdrawn.

After the injections, the craniotomy was filled with bone wax, the wound was sutured with cyanoacrylate (Vetbond, 3M, USA), and the animals were given buprenorphine (0.012 mg/kg i.m.) as an analgesic. After a recovery period of 3-5 days for zebra finches and pigeons, or 2 days for hummingbirds, birds were deeply anesthetized (ketamine/xylazine mixture i.m.) and transcardially perfused with saline (0.9 % NaCl) and 4% paraformaldehyde in 0.1M phosphate buffer (pH 7.4). Brains were extracted and immersed in paraformaldehyde for at least 24 hours at 4°C. Subsequently, brains were cryoprotected in 30% sucrose in 0.01M phosphate buffered saline (PBS, pH 7.4). Next, the brains were embedded in gelatin and again cryoprotected in 30% sucrose in PBS overnight. Using a freezing stage microtome, brains were sectioned in the coronal plane (40 μm sections) through the cerebellum and rostral extent of the pretectum, and sections were stored in individual wells containing PBS.

Antibody characterization.

Detailed information for the antibodies used in this study can be found in Table 1. The primary antibody was a rabbit polyclonal anti-calretinin previously characterized in

Western blots and immunohistochemical assays, and was shown to specifically recognize calretinin from tissues of multiple species (Schwaller et al., 1993). Furthermore, this antibody has been validated previously in the species used in this study (Wylie et al., 2008; Iwaniuk et al., 2009; Gutierrez-Ibanez et al., 2018).

Immunohistochemistry.

Immunohistochemical labelling for calretinin (CR) and Nissl staining with thionin aided the identification of structures and borders in the pretectum. Free-floating brain sections were washed five times in 0.01M PBS and blocked with 10% normal donkey serum (Jackson Immunoresearch Laboratories, West Grove, PA) and 0.4% Triton X-100 in PBS for 1 h at room temperature. Sections were then incubated for 48 h at 4°C in PBS containing 2.5% normal donkey serum, 0.4% Triton X-100 and a rabbit polyclonal antibody for CR (see Table 1; 1:2000; Swant Inc., Switzerland; immunogen: recombinant human calretinin; rabbit polyclonal, Cat-#7697, RRID: AB_2721226). Sections were washed in PBS and then incubated in PBS containing 2.5% normal donkey serum, 0.4% Triton X-100, and Alexa Fluor 488 (green)- or AMCA (blue)- conjugated donkey anti-rabbit IgG (H+L) (1:200, Jackson Immunoresearch Laboratories; Cat# 711-545-152, RRID: AB_2313584 and Cat# 711-155-152, RRID: AB_2340602 respectively) for 2 h at room temperature. Subsequently, the sections were rinsed in PBS and mounted on gelatinized slides for microscopy. After images of retrogradely labelled cells were acquired, we next stained the slides with thionin to confirm precise boundaries of the lateral and medial LM, and other pretectal nuclei.

Microscopy and image analysis.

Slide images were acquired on a compound light microscope (Leica DMRE) using a Retiga EXi *FAST* Cooled mono 12-bit camera (Qimaging, Burnaby, BC, Canada), and then analyzed with OPENLAB imaging software (Improvision, Lexington, MA, USA, RRID:rid_000096). Panoramic images were stitched together using PTGui (Rotterdam, Netherlands). Adobe Photoshop was used to compensate for brightness and contrast.

3. Results:

Comparative morphology of the pretectal region in nissl-stained sections.

For the nomenclature of the pretectal region, we adopted the detailed description of Gamlin and Cohen (Gamlin and Cohen, 1988a; b). In pigeons, the LM is divided into the lateral and medial subnuclei (LMl/LMm), which can be relatively easily distinguished in Nissl stained sections (Figure 1a-d). LMm is bordered medially by the nucleus laminaris precommisuralis (LPC), a crescent of darkly stained neurons (Figure 1a). The LPC and LMm appear contiguous with the external and internal layers of the ventral leaflet of the lateral geniculate nucleus (Glv) (Figure 1a,b). Medial to the LPC is the nucleus principalis precommisuralis (PPC), a pale region just lateral to nucleus rotundus (nRt) (Figure 1a,b). Caudally, the LMl merges into the rostral tectal gray (GTr), which contains small darkly stained cells that appear continuous with tectal layer five. The caudal tectal gray (GTc) appears darker in Nissl stain, with more densely packed cells, and is continuous with tectal layer eight. Although optic flow-sensitive cells have been attributed to LMl and LMm, the function of these other pretectal areas is unknown, though they are also retinal-recipient (Gamlin and Cohen, 1988b). The pretectal layers were readily distinguishable in zebra finches (Figure 1e-h) and hummingbirds (Figure 1i-l) from examination of Nissl stained sections.

Calretinin expression in the pretectal region.

Another tool we used to distinguish the layers in the pretectal region was calretinin (CR) expression. Previously, we have shown in pigeons that the LMm appears continuous with the internal layer of Glv, with light staining in the neuropil (Pakan et al., 2006; Iwaniuk et al., 2009). In both LMm and LMl, large multipolar neurons are CR immunopositive (CR+) (Gamlin and Cohen, 1988a; Iwaniuk et al., 2009). Additionally, we have shown that the projection from the LM to the cerebellum arises from large multipolar neurons, half of which are CR+ (Iwaniuk et al., 2009). CR immunoreactivity is generally absent in the LPC and PPC in pigeons. In hummingbirds, CR immunoreactivity is slightly different (Figure 3g,h). Similar to pigeons, CR+ cells are seen in the hummingbird LMl and there is light CR immunoreactivity in the neuropil of LMm, such that it appears continuous with the Glv. Compared to pigeon, there are fewer large CR+ cells in the hummingbird LMm. Also unlike the pigeon, CR+ neurons are observed in the LPC, and occasionally the PPC of hummingbirds. CR immunoreactivity

in the pretectal region of zebra finches resembles that of hummingbirds more so than pigeons (not shown).

Retrograde labeling from injections in the cerebellum.

Our description of retrograde labeling in the pretectal region from injections in the cerebellum is based on 8 cases, as outlined in Table 2. Figure 2 shows some of the injections of retrograde tracer in the cerebellum. The intent was to retrogradely label neurons that project as mossy fibers to the granular layer. As expected, extensive labeling was seen in the pretectal region and nBOR (see below). Additionally, and consistent with previous studies, some labeling was also seen in the medial spiriform nucleus and the pontine nuclei after injections in the oculomotor cerebellum, but not the vestibulocerebellum (Clarke, 1977; Wild, 1992; Pakan et al., 2006). A few retrogradely labeled neurons where seen in the vestibular nuclei complex and the cerebellar nuclei (Pakan et al., 2008). Invariably the injections included the molecular layer, thus, labeling was seen in the inferior olive. Consistent with previous studies (Gamlin and Cohen, 1988b; Lau et al., 1998; Wylie et al., 1999; Crowder et al., 2000; Pakan et al., 2005, 2006) from injections in the oculomotor cerebellum, retrogradely labeled cells were seen in the dorsal lamella and/or the ventral lamella of the inferior olive (Figure 2f), whereas from injections in IXcd (vestibulocerebellum), retrogradely labeled cells were found in the medial column of the inferior olive (Figure 2g).

Because the goal was to assign cells to the different pretectal layers, we developed a process illustrated in Figure 3. Using fluorescence microscopy, CR+ and retrogradely labeled cells were visualized and photomicrographs were obtained (Figure 3b,c,e,f,h). Subsequently, sections were Nissl stained to aid identification of the borders of pretectal regions (Figure 3a,d,g) and super-imposed on the fluorescent images. The number of cells in each region was then tabulated (Figure 3i-k). Figure 4 shows representative examples of retrogradely labeled cells in the pretectum and nBOR.

Differential labeling in the pretectum and nBOR from injections in IXcd and VI/VII.

The location of retrogradely labeled cells is shown in drawings of serial coronal sections through the midbrain. Figure 5 illustrates labeling resulting from injections in

folium IXcd (vestibulocerebellum) in pigeons, zebra finches, and hummingbirds. For all three species, and as previously shown in pigeons, retrogradely cells were found in the nBOR and pretectum (Brauth and Karten, 1977; Brecha et al., 1980; Pakan et al., 2006). Within the pretectum, the majority of these cells are located within the LMl.

Figure 6 illustrates retrograde labeling following injections in folia VI/VII (oculomotor cerebellum). For all three species, and as previously shown in pigeons, retrogradely cells were found in the nBOR and pretectum (Gamlin and Cohen, 1988b; Pakan et al., 2005; Wylie et al., 2007). However, there were differences between species with respect to labeling within pretectal regions. In pigeons, the majority of labeling was in LMm, while in hummingbirds and zebra finches there was much more labeling in the LPC and PPC.

In all three species, we quantify the proportion of retrogradely labeled cells in the nBOR and pretectum from injections in folium IXcd (vestibulocerebellum) and folia VI/VII (oculomotor cerebellum) (Figure 7, see Table 3 for cell counts). With respect to IXcd (vestibulocerebellum), hummingbirds have a greater proportion of inputs originating from the nBOR (73.7%) than the pretectum (26.3%), compared to zebra finches (36.3% from nBOR) and pigeons (51.7% from nBOR). With regard to folia VI/VII (oculomotor cerebellum), all species receive a greater proportion of input from the pretectum. Although, this is clearly higher in zebra finches (96.1%) compared to hummingbirds (77.3%) and pigeons (75.0%). Within the pretectum, clear differences in the pretectal-IXcd (vestibulocerebellum) projections were apparent across species (Figure 8, see Table 3 for cell counts). In hummingbirds, the vast majority of the pretectal cells projecting to folium IXcd were LMl cells (97.5%). Whereas a greater proportion of the pretectal cells projecting to IXcd arose from LMl in all three species, the proportion is markedly less in zebra finches (56.2%) and pigeons (65.1%). With respect to folia VI/VII (oculomotor cerebellum), in pigeons, a majority of the pretectal inputs arise from LMm (69.8%). Conversely, very few pretectal inputs to VI/VII (oculomotor cerebellum) arise from LMm in zebra finches (7.7%) and hummingbirds (8.0%). Furthermore, in hummingbirds and zebra finches a greater proportion of the pretectal inputs arise from

the LPC and PPC (hummingbirds: LPC: 19.3%, PPC: 31.9%; zebra finches: LPC: 27.4%, PPC: 46.5%).

4. Discussion:

Here we examined the proportions of projections from the nBOR and pretectum to the cerebellum in three different species of birds. The nBOR and LM process optic flow information resulting from self-motion and project to two distinct areas of the cerebellum: folium IXcd of the vestibulocerebellum and folia VI-VIII of the oculomotor cerebellum (Clarke, 1977; Brecha et al., 1980; Voogd and Barmack, 2006). The pathway to IXcd provides the optokinetic input mediating retinal stabilization (Pakan et al., 2006; Wylie, 2013; Wylie et al., 2018). In contrast, the inputs to folia VI-VIII are likely to integrate the global visual motion information, largely arising from the LM, with local motion cues from tectal-pontine pathways (Clarke, 1977; Brecha et al., 1980; Hellmann et al., 2004; Pakan and Wylie, 2006; Wylie et al., 2018). In this study we show clear differences in these projections between three species with different flight modes. Namely, within the pretectum, the majority of VI/VII-projecting cells arise from LMm in pigeons, while in hummingbirds and zebra finches a greater proportion of these cells arise from the LPC and PPC.

Hummingbirds display unique behaviors and have specialized features within their visual system, making them a powerful model for investigating the role of visual motion processing in avian flight guidance. Previous studies have established that the hummingbird LM is hypertrophied relative to other visual nuclei, that neurons in this nucleus prefer high velocity visual motion, and unlike other tetrapods, hummingbird LM cells do not exhibit a strong population-level bias for forward visual motion (Iwaniuk and Wylie, 2007; Gaede et al., 2017; Ibbotson, 2017).

Given that there are lateral and medial subdivisions within the LM, it is possible that one subdivision is primarily responsible for the hypertrophy observed in the hummingbird LM, and that this imbalance is reflected in projections to the cerebellum. In other avian species, the LMl is associated with slow velocities and a preference for forward motion and LMm cells prefer up, down or backward motion and high velocities

(Winterson and Brauth, 1985; Gamlin and Cohen, 1988a). This distinction is noteworthy because the LMl and LMm project to different regions of the cerebellum. Given that the hummingbird LM does not exhibit a strong population-level preference for forward motion (Gaede et al., 2017) – direction preference is more uniformly represented compared to other species – we expect that it is the LMm that is hypertrophied in hummingbirds, rather than the LMl (reviewed in Wylie et al., 2018). The LMm may be hypertrophied to support increased processing demands associated with the pathway to the oculomotor cerebellum (VI-VIII), and generated as hummingbirds fly through cluttered environments while feeding. Thus, if we were to expect a difference in cerebellar projections in hovering and non-hovering species, it would be with respect to the magnitude of projections from the LMm to the oculomotor cerebellum. Future investigation is required to elucidate the functional neuroanatomy of the LMm in hummingbirds. Further study using an anterograde tract tracer injected solely within the boundaries of the LMm could serve to demonstrate the locations of LMm efferent terminals.

Increased size and lamination of brain structures is associated with more complex processing capabilities (Pubols Jr et al., 1965; Pubols Jr and Pubols, 1972; Jerison, 1973; Finger, 1997; Barton, 1998; Reiner et al., 1998; Striedter, 2005). In this study, we show that the LPC and PPC, rather than the LMm, provide the majority of pretectal input to the oculomotor cerebellum in hummingbirds and zebra finches. In contrast, in pigeons, the largest pretectal input to the oculomotor cerebellum is from the LMm. This surprising result suggests that the LPC and PPC may be additional laminae of the LM in hummingbirds and zebra finches; such a finding may mean that the hummingbird and zebra finch LM are more laminated than that of the pigeon, indicating more sophisticated processing in these species. The relationship between increased lamination and more complex function is paralleled in other avian brain structures, namely the isthmo-optic nucleus (ION) and the nucleus isthmi magnocellularis (Imc) (Sohal and Narayanan, 1975; Repérant et al., 1989; Uchiyama, 1999; Faunes et al., 2013). For example, the ION is larger and has a more complex organization in songbirds, pigeons and hummingbirds than many other taxa (Repérant et al., 1989; Gutiérrez-Ibáñez et al., 2012). Gutiérrez-Ibáñez et al. (2012) propose that this structural difference supports the more complex

processing needs of visually-guided foraging behavior, aiding attention-switching between two parts of the retina (e.g. between myopic and emmetropic regions), allowing shifts between near- and long-range vision (Gutiérrez-Ibáñez et al., 2012).

The idea that the LPC and PPC are laminae of the LM in hummingbirds and zebra finches is further supported by the fact that at least some of the cerebellar-projecting neurons in the LPC/PPC are CR+. Large multipolar neurons in the LMm and LMl are CR+, while LPC and PPC neurons in many species lack CR labeling. Perhaps the presence of CR immunolabeling in hummingbirds and zebra finches indicates a migration of CR+ neurons from the LMm to the LPC and PPC. Given that in pigeons and other birds, the LM, but not the LPC or PPC, receives direct inputs from the retina (Gamlin and Cohen, 1988a; Krabichler et al., 2015), this proposed migration raises the question of whether the LMm in hummingbirds and zebra finches is now composed of interneurons doing more sophisticated processing. Alternatively, a migration of cells from LMm to LPC or PPC may not be indicative of changes in connectivity. For example, Vega-Zuniga et al. (2016) found that some cells in the LPC of chickens extend their dendrites into LMm, leading to the possibility that CR+ cells in the LPC of zebra finches and hummingbirds might still be retino-recipient (Vega-Zuniga et al., 2016). Additionally, the LPC and LMm share several inputs, including inputs from the ventral geniculate nucleus (GLv) and the adjacent nucleus intercalatus thalami (ICT; Vega-Zuniga et al., 2016, 2018), as well as the visual wulst (Wylie et al., 2005). This suggests a functional link among these regions, but further study of the functional response properties of LPC and LMm neurons is required.

To establish whether CR+ neurons in the LPC and PPC of hummingbirds and zebra finches are retino-recipient, further tracing studies examining retinal projections to the pretectum in these species is required. Little is known regarding the functional role of the LPC and PPC, though Gamlin and Cohen (1988) have shown that a small number of LM projections terminate in the pigeon PPC. Visual motion processing demands are likely to differ in birds with diverse flight behaviors, and this may be reflected in the functional neuroanatomy of each species. Further investigation examining the responses

of LPC and PPC neurons to visual motion may elucidate the roles of these nuclei in visuomotor processing in birds with different flight strategies.

Pakan and Wylie's (2006) initial study on pigeons had a larger dataset examining pretectal projections to the cerebellum. This included injections restricted to both the medial and lateral areas in both the oculomotor cerebellum and vestibulocerebellum. Although LMm projects primarily to the oculomotor cerebellum, and the LMl projects mainly to the vestibulocerebellum, no other topography was observed. Furthermore, small, localized injections of anterograde tracer in the nBOR and LM resulted in mossy fiber terminals through a broad extent rostrocaudally and mediolaterally in folium IXcd (Pakan et al., 2010). Previous studies in pigeon have shown low between-animal variability after retrograde tracer injections in the oculomotor cerebellum (VI-VIII) and vestibulocerebellum (IXcd) (Pakan and Wylie, 2006). Because the current study employed similar techniques in the same brain regions, we did not expect to observe significant between-animal variability. Furthermore the projection patterns observed in pigeon in this study mirror those observed by Pakan and Wylie (2006).

A perplexing problem presented by the findings of this study is that pretectal projections to the oculomotor cerebellum in zebra finches look similar to that of hummingbirds – a result that was not expected. Anna's hummingbirds have an average wingbeat frequency of ~34-45 Hz (Kim et al., 2014; Tobalske, 2016) and zebra finches also have a relatively high wingbeat frequency of 27-30 Hz during forward flight (Tobalske et al., 2005; Donovan et al., 2013). In contrast, pigeons have a much lower average wingbeat frequency (6-7 Hz) during forward flight (Berg and Biewener, 2010). A possible explanation for the differences observed between projections to the oculomotor cerebellum in zebra finches and hummingbirds versus pigeons is this disparity between wingbeat frequencies and associated visuomotor processing demands. Other distinctions between these two groups include their size, habitat and flight behavior. Hummingbirds and zebra finches are substantially smaller than pigeons; Anna's hummingbirds have a mass of ~3-4 g, zebra finches weigh ~12-15 g, and pigeons typically weigh ~350-400 g. Hummingbirds exhibit dynamic flight modes including hovering and high-speed displays (Altshuler and Dudley, 2002), and zebra finches use a unique flap-bounding flight at all

359 speeds. When combined with our anatomical results, these kinematic studies suggest a
360 relationship between bird size, the processing demands of unique flight behaviors, and
361 increased lamination within the pretectum. Testing this hypothesis will require
362 investigation of the morphology and function of these pretectal regions.

References:

Altshuler DL, Dudley R. 2002. The ecological and evolutionary interface of hummingbird flight physiology. J Exp Biol 205:2325–2336.

Barton RA. 1998. Visual specialization and brain evolution in primates. Proc R Soc Lond B Biol Sci 265:1933–1937.

Berg AM, Biewener AA. 2010. Wing and body kinematics of takeoff and landing flight in the pigeon (*Columba livia*). J Exp Biol 213:1651–1658.

Brauth SE, Karten HJ. 1977. Direct accessory optic projections to the vestibulo-cerebellum: a possible channel for oculomotor control systems. Exp Brain Res 28:73–84.

Brecha N, Karten HJ, Hunt SP. 1980. Projections of the nucleus of the basal optic root in the pigeon: An autoradiographic and horseradish peroxidase study. J Comp Neurol 189:615–670.

Clarke PGH. 1977. Some visual and other connections to the cerebellum of the pigeon. J Comp Neurol 174:535–552.

Crowder NA, Winship IR, Wylie DR. 2000. Topographic organization of inferior olive cells projecting to translational zones in the vestibulocerebellum of pigeons. J Comp Neurol 419:87–95.

Donovan ER, Keeney BK, Kung E, Makan S, Wild JM, Altshuler DL. 2013. Muscle activation patterns and motor anatomy of Anna's hummingbirds *Calypte anna* and zebra finches *Taeniopygia guttata*. Physiol Biochem Zool Ecol Evol Approaches 86:27–46.

Faunes M, Fernández S, Gutiérrez-Ibáñez C, Iwaniuk AN, Wylie DR, Mpodozis J, Karten HJ, Marín G. 2013. Laminar segregation of GABAergic neurons in the avian nucleus isthmi pars magnocellularis: a retrograde tracer and comparative study. J Comp Neurol 521:1727–1742.

Finger TE. 1997. Feeding patterns and brain evolution in ostariophysean fishes. Acta Physiol Scand Suppl 638:59–66.

Fite KV. 1985. Pretectal and Accessory-Optic Visual Nuclei of Fish, Amphibia and Reptiles: Theme and Variations (Part 1 of 2). Brain Behav Evol 26:71–80.

Gaede AH, Goller B, Lam JP, Wylie DR, Altshuler DL. 2017. Neurons responsive to global visual motion have unique tuning properties in hummingbirds. Curr Biol 27:279–285.

Gamlin PD, Cohen DH. 1988a. Projections of the retinorecipient pretectal nuclei in the pigeon (*Columba livia*). J Comp Neurol 269:18–46.

398 Gamlin PD, Cohen DH. 1988b. Retinal projections to the pretectum in the pigeon
399 (*Columba livia*). J Comp Neurol 269:1–17.

400 Giolli RA, Blanks RH, Lui F. 2006. The accessory optic system: basic organization with
401 an update on connectivity, neurochemistry, and function. Prog Brain Res
402 151:407–440.

403 Goller B, Altshuler DL. 2014. Hummingbirds control hovering flight by stabilizing visual
404 motion. Proc Natl Acad Sci 111:18375–18380.

405 Gutierrez-Ibanez C, Gaede AH, Dannish MR, Altshuler DL, Wylie DR. 2018. The retinal
406 projection to the nucleus lentiformis mesencephali in zebra finch (*Taeniopygia*
407 *guttata*) and Anna's hummingbird (*Calypte anna*). J Comp Physiol A 204:369–
408 376.

409 Gutiérrez-Ibáñez C, Iwaniuk AN, Lisney TJ, Faunes M, Marín GJ, Wylie DR. 2012.
410 Functional implications of species differences in the size and morphology of the
411 isthmo optic nucleus (ION) in birds. PloS One 7:e37816.

412 Hellmann B, Güntürkün O, Manns M. 2004. Tectal mosaic: organization of the
413 descending tectal projections in comparison to the ascending tectofugal pathway
414 in the pigeon. J Comp Neurol 472:395–410.

415 Hoffmann K-P, Schoppmann A. 1981. A quantitative analysis of the direction-specific
416 response of neurons in the cat's nucleus of the optic tract. Exp Brain Res 42:146–
417 157.

418 Ibbotson MR. 2017. Visual neuroscience: unique neural system for flight stabilization in
419 hummingbirds. Curr Biol 27:R58–R61.

420 Ibbotson MR, Mark RF, Maddess TL. 1994. Spatiotemporal response properties of
421 direction-selective neurons in the nucleus of the optic tract and dorsal terminal
422 nucleus of the wallaby, *Macropus eugenii*. J Neurophysiol 72:2927–2943.

423 Iwaniuk AN, Pakan JM, Gutiérrez-Ibáñez C, Wylie DR. 2009. Expression of calcium-
424 binding proteins in cerebellar-and inferior olivary-projecting neurons in the
425 nucleus lentiformis mesencephali of pigeons. Vis Neurosci 26:341–347.

426 Iwaniuk AN, Wylie DRW. 2007. Neural specialization for hovering in hummingbirds:
427 Hypertrophy of the pretectal nucleus lentiformis mesencephali. J Comp Neurol
428 500:211–221.

429 Jerison HJ. 1973. Evolution of the brain and intelligence. Acad Press.

430 Kim EJ, Wolf M, Ortega-Jimenez VM, Cheng SH, Dudley R. 2014. Hovering
431 performance of Anna's hummingbirds (*Calypte anna*) in ground effect. J R Soc
432 Interface 11:20140505.

Krabichler Q, Vega-Zuniga T, Morales C, Luksch H, Marín GJ. 2015. The visual system of a Palaeognathous bird: Visual field, retinal topography and retino-central connections in the Chilean Tinamou (*Nothoprocta perdicaria*). J Comp Neurol 523:226–250.

Lau KL, Glover RG, Linkenhoker B, Wylie DRW. 1998. Topographical organization of inferior olive cells projecting to translation and rotation zones in the vestibulocerebellum of pigeons. Neuroscience 85:605–614.

Mckenna OC, Wallman J. 1985. Accessory optic system and pretectum of birds: Comparisons with those of other vertebrates. Brain Behav Evol 26:91–116.

Mustari MJ, Fuchs AF. 1990. Discharge patterns of neurons in the pretectal nucleus of the optic tract (NOT) in the behaving primate. J Neurophysiol 64:77–90.

Pakan JM, Graham DJ, Iwaniuk AN, Wylie DR. 2008. Differential projections from the vestibular nuclei to the flocculus and uvula-nodulus in pigeons (*Columba livia*). J Comp Neurol 508:402–417.

Pakan JM, Graham DJ, Wylie DR. 2010. Organization of visual mossy fiber projections and zebrin expression in the pigeon vestibulocerebellum. J Comp Neurol 518:175–198.

Pakan JM, Krueger K, Kelcher E, Cooper S, Todd KG, Wylie DR. 2006. Projections of the nucleus lentiformis mesencephali in pigeons (*Columba livia*): a comparison of the morphology and distribution of neurons with different efferent projections. J Comp Neurol 495:84–99.

Pakan JM, Todd KG, Nguyen AP, Winship IR, Hurd PL, Jantzie LL, Wylie DR. 2005. Inferior olivary neurons innervate multiple zones of the flocculus in pigeons (*Columba livia*). J Comp Neurol 486:159–168.

Pakan JM, Wylie DR. 2006. Two optic flow pathways from the pretectal nucleus lentiformis mesencephali to the cerebellum in pigeons (*Columba livia*). J Comp Neurol 499:732–744.

Pubols Jr BH, Pubols LM. 1972. Neural organization of somatic sensory representation in the spider monkey. Brain Behav Evol 5:342–366.

Pubols Jr BH, Welker WI, Johnson Jr JI. 1965. Somatic sensory representation of forelimb in dorsal root fibers of raccoon, coatimundi, and cat. J Neurophysiol 28:312–341.

Reiner A, Medina L, Veenman CL. 1998. Structural and functional evolution of the basal ganglia in vertebrates. Brain Res Rev 28:235–285.

Repérant J, Miceli D, Vesselkin NP, Molotchnikoff S. 1989. The centrifugal visual system of vertebrates: a century-old search reviewed. In: International Review of Cytology. Vol. 118. Elsevier. p 115–171.

Schwaller B, Buchwald P, Blümcke I, Celio MR, Hunziker W. 1993. Characterization of a polyclonal antiserum against the purified human recombinant calcium binding protein calretinin. Cell Calcium 14:639–648.

Simpson JI. 1984. The accessory optic system. Annu Rev Neurosci 7:13–41.

Sohal GS, Narayanan CH. 1975. Effects of optic primordium removal on the development of the isthmo-optic nucleus in the duck (*Anas platyrhynchos*). Exp Neurol 46:521–533.

Striedter GF. 2005. Principles of Brain Evolution (Sinauer, Sunderland, MA).

Tobalske BW. 2016. Evolution of avian flight: muscles and constraints on performance. Philos Trans R Soc B Biol Sci 371.

Tobalske BW, Puccinelli LA, Sheridan DC. 2005. Contractile activity of the pectoralis in the zebra finch according to mode and velocity of flap-bounding flight. J Exp Biol 208:2895–2901.

Uchiyama H. 1999. The isthmo-optic nucleus: A possible neural substrate for visual competition. Neurocomputing 26:565–571.

Vega-Zuniga T, Marín G, González-Cabrera C, Planitscher E, Hartmann A, Marks V, Mpodozis J, Luksch H. 2016. Microconnectomics of the pretectum and ventral thalamus in the chicken (*Gallus gallus*). J Comp Neurol 524:2208–2229.

Vega-Zuniga T, Trost D, Schicker K, Bogner EM, Luksch H. 2018. The medial ventrothalamic circuitry: cells implicated in a bimodal network. Front Neural Circuits 12:9.

Voogd J, Barmack NH. 2006. Oculomotor cerebellum. Prog Brain Res 151:231–268.

Waespe W, Henn V. 1987. Gaze stabilization in the primate. The interaction of the vestibulo-ocular reflex, optokinetic nystagmus, and smooth pursuit. Rev Physiol Biochem Pharmacol 106:37–125.

Wild JM. 1992. Direct and indirect “cortico”-rubral and rubro-cerebellar cortical projections in the pigeon. J Comp Neurol 326:623–636.

Winterson BJ, Brauth SE. 1985. Direction-selective single units in the nucleus lentiformis mesencephali of the pigeon (*Columba livia*). Exp Brain Res 60:215–226.

Wylie DR. 2013. Processing of visual signals related to self-motion in the cerebellum of pigeons. Front Behav Neurosci 7.

Wylie DR, Crowder NA. 2000. Spatiotemporal properties of fast and slow neurons in the pretectal nucleus lentiformis mesencephali in pigeons. J Neurophysiol 84:2529–2540.

Wylie DR, Gutiérrez-Ibáñez C, Gaede AH, Altshuler DL, Iwaniuk AN. 2018. Visual-cerebellar pathways and their roles in the control of avian flight. Front Neurosci 12.

Wylie DR, Ogilvie CJ, Crowder NA, Barkley RR, Winship IR. 2005. Telencephalic projections to the nucleus of the basal optic root and pretectal nucleus lentiformis mesencephali in pigeons. Vis Neurosci 22:237–247.

Wylie DR, Pakan JM, Elliott CA, Graham DJ, Iwaniuk AN. 2007. Projections of the nucleus of the basal optic root in pigeons (*Columba livia*): a comparison of the morphology and distribution of neurons with different efferent projections. Vis Neurosci 24:691–707.

Wylie DR, Winship IR, Glover RG. 1999. Projections from the medial column of the inferior olive to different classes of rotation-sensitive Purkinje cells in the flocculus of pigeons. Neurosci Lett 268:97–100.

Wylie DRW, Pakan JMP, Gutiérrez-Ibáñez C, Iwaniuk AN. 2008. Expression of calcium-binding proteins in pathways from the nucleus of the basal optic root to the cerebellum in pigeons. Vis Neurosci 25:701–707.

Figure Legends:

Figure 1:
Nissl-stained coronal brain sections through the midbrain, presented anterior to posterior. **a-d**: pigeon midbrain sections, scale bar = 1 mm. **e-h**: zebra finch midbrain sections, scale bar = 500 µm. **i-l**: hummingbird midbrain sections, scale bar = 500 µm. Line drawings illustrate the borders of relevant nuclei. Nissl staining was used to confirm the borders of midbrain nuclei.

Glv = ventral lateral geniculate nucleus, **GTc** = caudal tectal gray, **GTr** = rostral tectal gray, **IOT** = tractus isthmo-opticus, **LMl** lentiformis pars lateralis, **LMm** = lentiformis mesencephali pars medialis, **LPC** = nucleus laminaris precommisuralis, **nRt** = nucleus rotundus, **PPC** = nucleus principalis precommisuralis, **PT** = pretectal nucleus, **SP** = nucleus subpretectalis, **SpL** = lateral spiriform nucleus, **SpM** = medial spririform nucleus, **TeO** = optic tectum

Figure 2:
Photomicrographs showing injection sites in the oculomotor cerebellum (folia VI/VII) or the vestibulocerebellum (folium IXcd). The neuronal tracer cholera toxin B (CTB)-Alexa Fluor 488 (green injection sites) or 594 (red injection sites) was injected using iontophoresis. Sections were counter-stained with calretinin to better visualize the injection site. **a-b**: Injections in the hummingbird vestibulocerebellum (folium IXcd) (a) and the oculomotor cerebellum (folium VI) (b). **c-d**: Injections in the zebra finch oculomotor cerebellum (folium VI) (c) and vestibulocerebellum (folium IXcd) (d). **e**: Injection into the pigeon oculomotor cerebellum (folium VI). **f-g**: Retrograde labeling in the inferior olive is confirmation that the tracer transported successfully. Cells in the lateral inferior olive project to the oculomotor cerebellum (folia VI-VIII). (f) Photomicrograph showing retrograde labeling in the dorsal lamella and/or the ventral lamella of the inferior olive of a hummingbird after injection in folium VI. Cells in the medial column of the inferior olive (mcIO) project to the vestibulocerebellum (folium IXcd). (g) Photomicrograph showing retrograde labeling in the mcIO of a zebra finch after injection in folium IXcd.

Figure 3:
Cells within the different pretectal layers were identified using a process in which retrogradely labeled cells and calretinin-positive cells were first visualized using fluorescence microscopy. Next, sections were Nissl stained to aid identification of brain nuclei. **a-c:** Images of Nissl stained sections in the pretectum of pigeon (a) were combined with fluorescence imaging of calretinin-positive cells (b) to identify the borders of pretectal nuclei (c). Borders defined using Nissl stained sections are overlaid on photomicrographs showing calretinin expression; shown in panel c. c is the inset in b. **d-f:** Similarly, in zebra finches, Nissl stained sections (d) were used in conjunction with calretinin expression (e) to identify borders of pretectal layers (illustrated in panel f). **g-k:** In hummingbirds, images of Nissl stained sections (g) were combined with photomicrographs showing calretinin expression in the same sections (h). Photomicrographs of retrogradely labeled cells (i) were merged with border illustrations

created using merged calretinin expression and Nissl staining. Subsequently, the number of cells in each region was tabulated (i-k). k = inset in h-j. Arrows in k indicate retrogradely-labeled, calretinin-positive cells. Scale bars: e, f = 100 μm, k = 50 μm, all others = 200 μm.

Glv = ventral lateral geniculate nucleus, **GTr** = rostral tectal gray, **LMl** lentiformis pars lateralis, **LMm** = lentiformis mesencephali pars medialis, **LPC** = nucleus laminaris precommisuralis, **nRt** = nucleus rotundus, **PPC** = nucleus principalis precommisuralis, **TeO** = optic tectum

Figure 4:
Representative photomicrographs of calretinin (CR) expression and retrogradely labeled cells in the pretectum and nBOR. **a-h:** CR expression (a, e) and retrogradely labeled cells (b, f) in the LM of pigeon after neural tracer injections in folium VII. c: Merged image of (a) and (b). d = inset in c. g: Merged image of (e) and (f). h = inset in g. Scale bars = 100 μm for a-c, e-g. Scale bars in d and h are 50 μm. **i-k:** CR expression (i) and retrogradely labeled cells (j) in the zebra finch nBOR after injection in folium IXcd. k: Merged image of (i) and (j). Scale bar =100 μm. **l-n:** CR expression (i) and retrogradely labeled cells (m) in the hummingbird nBOR after injection in folium VI. n: Merged image of (l) and (m). Scale bars = 100 μm. **o-q:** CR expression (o) and retrogradely labeled cells (p) in the hummingbird LM after injection in folium VI. q: Merged image of (o) and (p). Scale bars = 100 μm.

Glv = ventral lateral geniculate nucleus, **LMl** lentiformis pars lateralis, **LMm** = lentiformis mesencephali pars medialis, **LPC** = nucleus laminaris precommisuralis, **nBOR** = nucleus of the basal optic root, **nRt** = nucleus rotundus, **PPC** = nucleus principalis precommisuralis

Figure 5:
Illustrations of retrogradely labeled cells after neural tracer microinjection in the vestibulocerebellum (folium IXcd). Drawings of coronal brain sections, ordered anterior to posterior, through the midbrain and nBOR. Red points indicate retrogradely labeled cell bodies. “Ipsi” and “Contra” indicate the panels that are ipsilateral or contralateral to the injection site, respectively. Pigeon: scale bars = 1 mm. Zebra finch: scale bars = 500 μm. Hummingbird: scale bars = 500 μm.

Glv = ventral lateral geniculate nucleus, **GT** = tectal gray, **GTc** = caudal tectal gray, **GTr** = rostral tectal gray, **Imc** = nucleus isthmi, pars magnocellularis, **IOT** = tractus isthmo-opticus, **Ipc** = nucleus isthmi, pars parvocellularis, **LMl** lentiformis pars lateralis, **LMm** = lentiformis mesencephali pars medialis, **LPC** = nucleus laminaris precommisuralis, **nBOR** = nucleus of the basal optic root, **nRt** = nucleus rotundus, **OT** = tractus opticus, **OV** = nucleus ovoidalis, **PPC** = nucleus principalis precommisuralis, **PT** = pretectal nucleus, **SP** = nucleus subpretectalis, **SpL** = lateral spiriform nucleus, **SpM** = medial spririform nucleus, **TeO** = optic tectum

Figure 6:

Illustrations of retrogradely labeled cells after neural tracer microinjection in the oculomotor cerebellum (folia VI-VIII). Drawings of coronal brain sections, ordered anterior to posterior, through the midbrain and nBOR. Red points indicate retrogradely labeled cell bodies. “Ipsi” and “Contra” indicate the panels that are ipsilateral or contralateral to the injection site, respectively. Pigeon: scale bars = 1 mm. Zebra finch: scale bars = 500 μm. Hummingbird: scale bars = 500 μm.

Glv = ventral lateral geniculate nucleus, **GT** = tectal gray, **GTc** = caudal tectal gray, **GTr** = rostral tectal gray, **Imc** = nucleus isthmi, pars magnocellularis, **IOT** = tractus isthmo-opticus, **LMl** lentiformis pars lateralis, **LMm** = lentiformis mesencephali pars medialis, **LPC** = nucleus laminaris precommisuralis, **nBOR** = nucleus of the basal optic root, **nRt** = nucleus rotundus, **OM** = tractus occipitomesencephalicus, **PPC** = nucleus principalis precommisuralis, **PT** = pretectal nucleus, **SP** = nucleus subpretectalis, **SpL** = lateral spiriform nucleus, **SpM** = medial spririform nucleus, **TeO** = optic tectum

Figure 7:
Pie charts illustrating the proportion of retrogradely labeled cells in the nBOR and pretectum from injections in the vestibulocerebellum (folium IXcd) and oculomotor cerebellum (folia VI/VII). See Table 3 for cell counts.

Figure 8:
Pie charts illustrating, within the pretectum, the proportion of retrogradely labeled cells in the lateral lentiformis mesencephali (LMl), medial lentiformis mesencephali (LMm), nucleus laminaris precommisuralis (LPC), and nucleus principalis precommisuralis (PPC) from injections in the vestibulocerebellum (folium IXcd) and oculomotor cerebellum (folia VI/VII). See Table 3 for cell counts.

Table 1: Summary of antibodies used.

	Antibody	Host/Isotype	Immunogen or target	Supplier	Catalog number, RRID	Concentration
Primary	Calretinin	Rabbit/polyclonal	Immunogen: Recombinant human calretinin	Swant Inc.,	Cat-#7697, RRID: AB_2721226	1:2000
Secondary	Alexa Fluor 488 donkey anti-rabbit IgG (H+L)	Donkey	Target: Rabbit IgG	Jackson Immunoresearch Laboratories	711-545-152, RRID: AB_2313584	1:200
Secondary	AMCA donkey anti-rabbit IgG (H+L)	Donkey	Target: Rabbit IgG	Jackson Immunoresearch Laboratories	711-155-152, RRID: AB_2340602	1:200

Table 2: Summary of cerebellum injections

Species	Folia Injected
Pigeon 1	IXcd
Pigeon 2	VI
Zebra Finch 1	IXcd
Zebra Finch 2	VI
Hummingbird 1	VI
Hummingbird 2	IXcd
Hummingbird 3	VI
Hummingbird 4	IXcd

Table 3: Summary of retrogradely labeled cell counts.

Species	Injection site	Total cells	nBOR	Pretectum total	LMl	LMm	LPC	PPC
Pigeon 1	IXcd	1334	689	645	420	149	61	15
Zebra Finch 1	IXcd	756	274	482	271	80	46	85
Hummingbird 2	IXcd	179	135	44	44	0	0	0
Hummingbird 4	IXcd	282	203	79	75	2	2	0
Pigeon 2	VI	455	114	341	76	238	20	7
Zebra Finch 2	VI	255	10	245	45	19	67	114
Hummingbird 1	VI	474	135	339	130	24	75	110
Hummingbird 3	VI	904	153	751	324	67	124	236

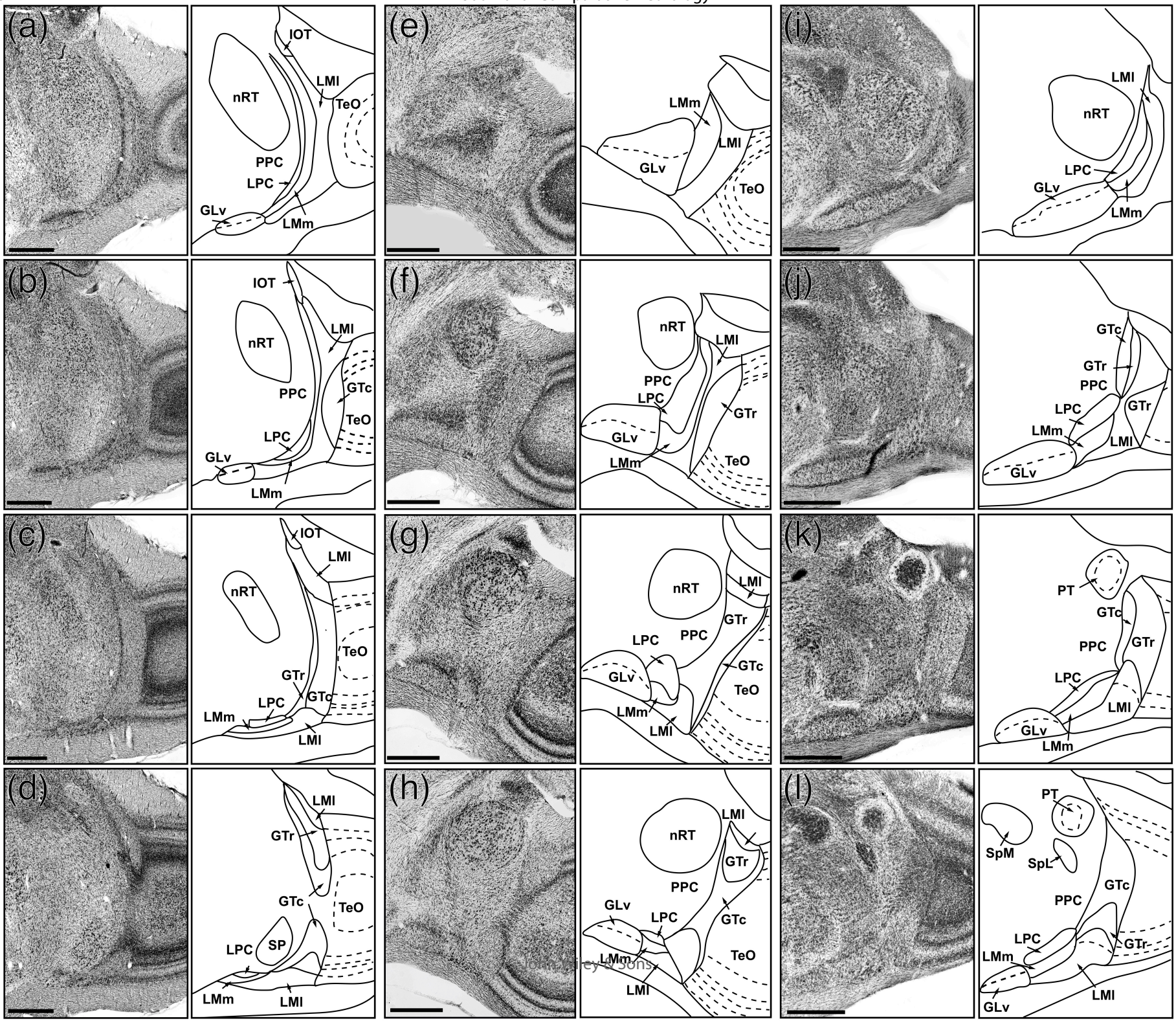

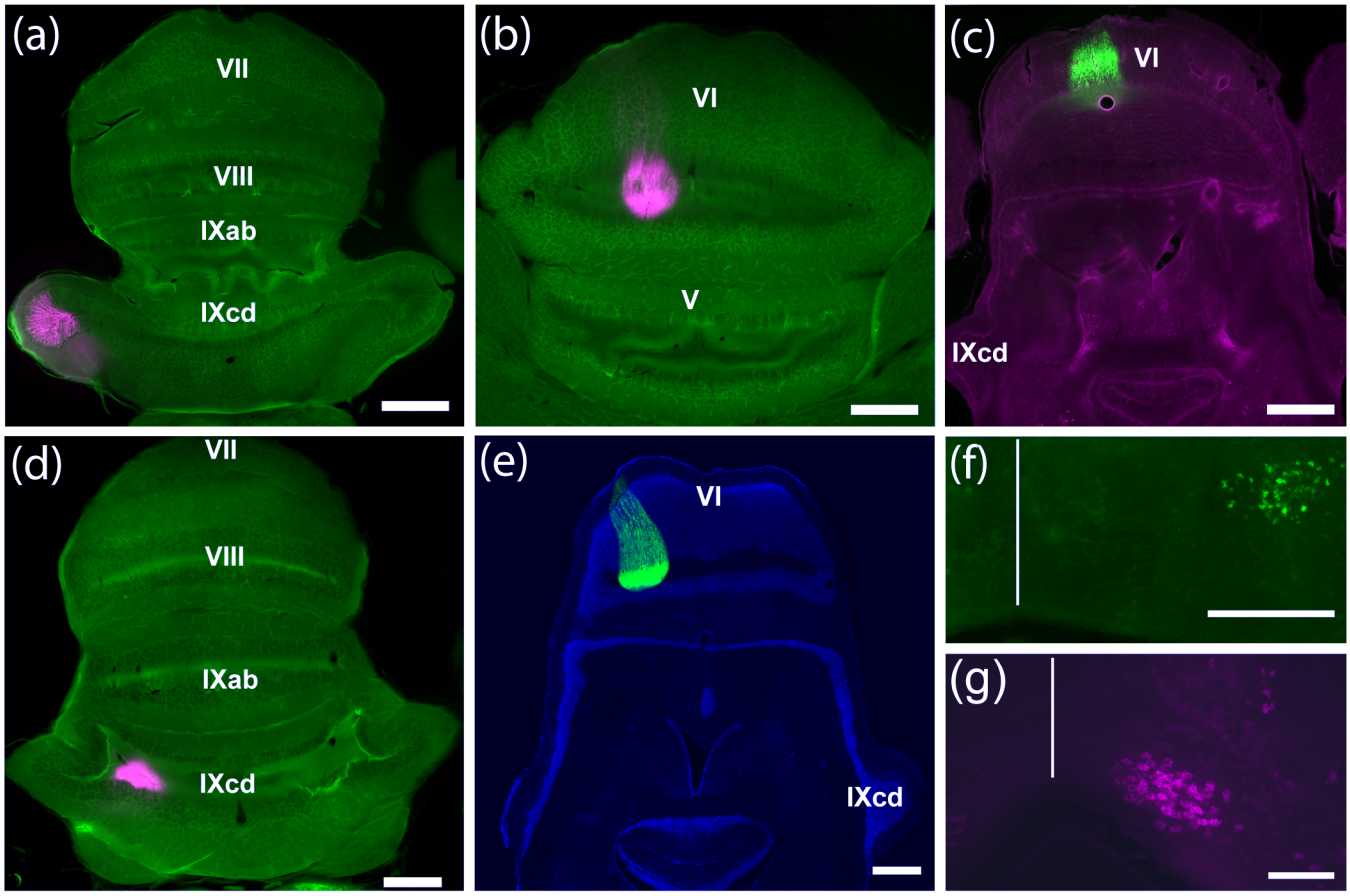
(a)
VII
VIII
IXab
IXcd
(b)
VI
V
(c)
VI
IXcd
(d)
VII
VIII
IXab
IXcd
(e)
VI
IXcd
(f)
(g)

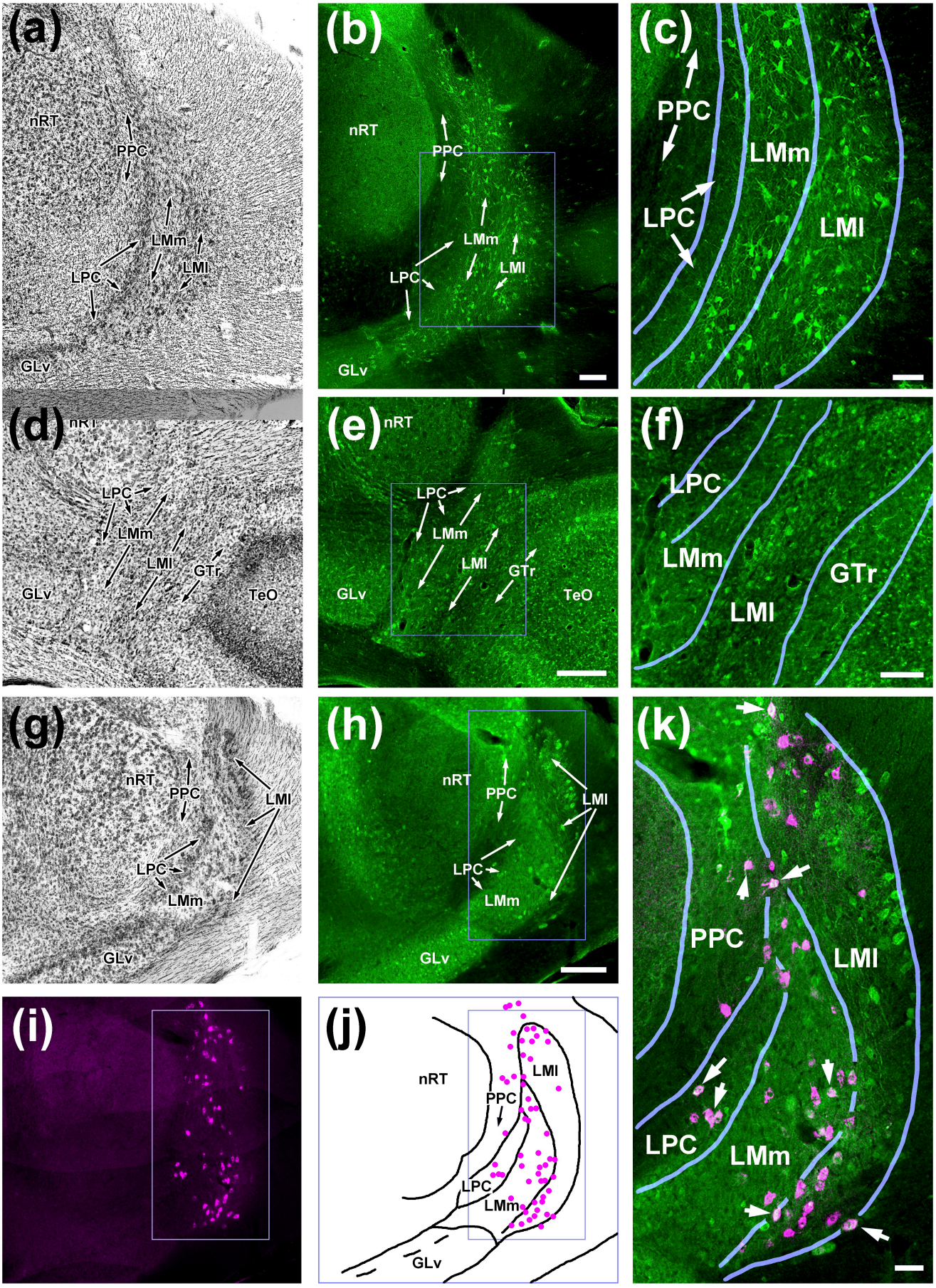
(a)
nRT
PPC
LMm
LMl
LPC
GLv
(b)
nRT
PPC
LMm
LMl
LPC
GLv
(c)
PPC
LMm
LPC
LMl
(d)
LPC
LMm
LMl
GTr
GLv
TeO
(e)
nRT
LPC
LMm
LMl
GTr
GLv
TeO
(f)
LPC
LMm
GTr
LMl
(g)
nRT
PPC
LMl
LPC
LMm
GLv
(h)
nRT
PPC
LMl
LPC
LMm
GLv
(k)
PPC
LMl
LPC
LMm
(i)
(j)
nRT
LMl
PPC
LPC
LMm
GLv

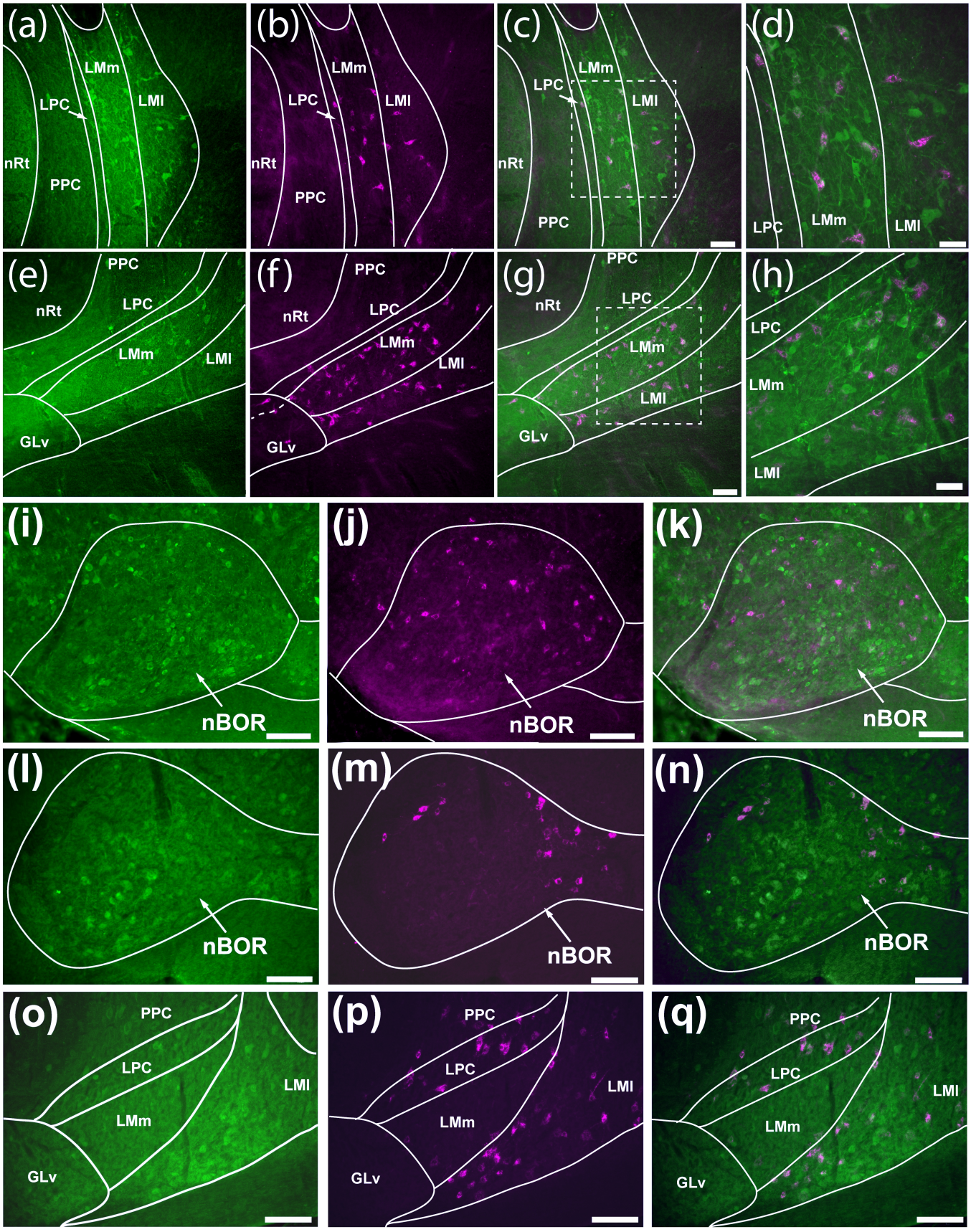
(a)
LMm
LPC
LMI
nRt
PPC
(b)
LMm
LPC
LMI
nRt
PPC
(c)
LMm
LPC
LMI
nRt
PPC
(d)
LPC
LMm
LMI
(e)
PPC
nRt
LPC
LMm
LMI
GLv
(f)
PPC
nRt
LPC
LMm
LMI
GLv
(g)
PPC
nRt
LPC
LMm
LMI
GLv
(h)
LPC
LMm
LMI
(i)
nBOR
(j)
nBOR
(k)
nBOR
(l)
nBOR
(m)
nBOR
(n)
nBOR
(o)
PPC
LPC
LMI
LMm
GLv
(p)
PPC
LPC
LMI
LMm
GLv
(q)
PPC
LPC
LMI
LMm
GLv